The interaction of oxygen with the Ag(110) surface

1996 J. Phys.: Condens. Matter 8 2247

(http://iopscience.iop.org/0953-8984/8/14/003)

J. Phys.: Condens. Matter **8** (1996) 2247–2263. Printed in the UK

The interaction of oxygen with the Ag(110) surface

Age Raukema, David A Butler and Aart W Kleyn

FOM-Institute for Atomic and Molecular Physics, Kruislaan 407, 1098 SJ Amsterdam, The Netherlands†

Received 24 November 1995, in final form 23 January 1996

Abstract. Results on the scattering and the dissociative sticking of O_2 molecules on the Ag(110) surface are presented. The dependence on the incidence energy and angle of the molecules is investigated by employing molecular beam techniques. Both the angle with respect to the surface normal and that with respect to the $\langle 1\bar{1}0\rangle$ azimuthal direction on the surface are varied. The $\langle 1\bar{1}0\rangle$ and $\langle 001\rangle$ azimuthal directions display a different corrugation as observed by the incident molecule. Dissociative sticking is observed to proceed via the molecular chemisorption state and is strongly enhanced by the incidence energy. An azimuthal dependence of the sticking is observed. Results on the desorption of O_2 from the Ag(110) surface are also given.

1. Introduction

By studying the fundamental properties of gas–surface reactions on well defined surfaces, insight can be gained into the mechanism of chemical reactions taking place at technologically important surfaces, for instance in catalysis. In such a practical situation, the surface will not be well defined, whereas in most fundamental studies a well characterized single crystal is used. Studying the gas–surface interaction of one gas with the different surface planes of one solid material may lead to more insight into the fundamental properties of the interaction. Changing the surface plane alters the geometric and electronic properties presented to the molecules: hence their role in the interaction can be addressed. The interaction of oxygen with the different surface planes of silver is a good candidate for such a comparative study.

The Ag(111) and Ag(110) surfaces have almost identical binding states for oxygen: a shallow physisorption state, a stronger molecular chemisorption state, an atomically adsorbed state and a subsurface one as has been recently reviewed by Besenbacher and Nørskov [1]. The charge transfer to the oxygen molecule in the molecular chemisorption state may be somewhat different for the two surfaces. Desorption measurements reveal almost identical desorption temperatures from these two surfaces for these different adsorption states and the same behaviour for oxygen adsorption may be expected. However, this is not the case. Adsorption measurements from an ambient gas show a difference of at least two orders of magnitude in both the molecular and the dissociative sticking probability with the sticking for the Ag(111) having the lowest probability, of the order of 10^{-7}–10^{-6} [2, 3, 4]. These measurements show a different reactivity with oxygen for the two surfaces and the question arises of whether oxygen adsorption occurs via similar processes on both surfaces or not.

† Fax: X-31-20-6684106; e-mail: kleyn@amolf.nl.

0953-8984/96/142247+17$19.50

We have already carried out a number of experiments addressing the interaction of O_2 with the Ag(111) surface using a supersonic molecular beam. Both sticking and scattering experiments were done. The scattering experiments showed a large increase in surface corrugation for normal-incidence energies exceeding a threshold energy of 0.2 eV [5]. Above the same threshold energy, transient trapping–desorption of O_2 at the Ag(111) surface was observed. It was suggested that this involved the trapping of oxygen molecules into the molecular chemisorption state without equilibration and a subsequent desorption of molecules [6, 7]. Transient trapping shows a maximum probability of approximately 30%. The incidence energy and angular dependence of the molecular chemisorption coefficient follows the transient trapping probability, but with a probability approximately three orders of magnitude lower. The dissociative sticking was seen to proceed via the molecular chemisorption state in a thermal process [8]. A direct process to dissociation was also observed, overtaking the precursor process at incidence energies E_i exceeding approximately 1 eV and for incidence angles θ_i close to the surface normal. The energy threshold observed for transient trapping and the population of the molecular chemisorption state is identical to the one found for the increased surface corrugation observed in scattering. It was suggested that a first step to molecular chemisorption is transient trapping followed by desorption or equilibration in the molecular chemisorption well.

The Ag(111) surface is relatively smooth with a hexagonal close-packed structure. The Ag(110) surface consists of rows of close-packed surface atoms in the $\langle 1\bar{1}0\rangle$ direction. This results in a strong surface corrugation in the $\langle 001\rangle$ direction. Molecular and dissociative sticking at the Ag(110) surface has been measured using a molecular beam by Vattuone *et al* [9, 10, 11, 12] and Rocca *et al* [13]. For this surface the dissociative sticking was also observed to proceed via the molecular chemisorption state. However, the population of the molecular chemisorption state occurred with a probability three orders of magnitude higher than on the Ag(111) surface. The dependence on E_i and θ_i seems almost identical for the two surfaces. Vattuone *et al* could not reach incidence energies over $E_i = 0.6$ eV and were therefore only able to observe an increase in the sticking of O_2 at the Ag(110) surface with increasing E_i. A saturation of the sticking coefficient with further increasing incidence energy or even a decrease after reaching a maximum value, such as we observed for the O_2–Ag(111) system, could not be reported. More information on the dependence on E_i and θ_i will certainly help in deriving a better physical picture of the adsorption process. The transient trapping of oxygen found at the Ag(111) surface may also play a role at the Ag(110) surface. Experiments on this matter are presented here.

Scattering experiments will also be discussed. From these measurements one obtains information on the energy transfer in the scattering process and on the degree of surface corrugation as experienced by the incident O_2 molecule. The existence of transient trapping and desorption from the molecular or atomic chemisorption state may also be visible in the time-of-flight (TOF) spectra recorded for the scattering experiments.

2. Experimental procedure

The experiments have been performed in a molecular beam machine described before [5] and shown in figure 1. Briefly, it consists of a triply differentially pumped molecular beam line connected to a UHV scattering chamber. The first stage contains the nozzle and the second stage of the beam line contains a chopper. Both a double-slit 0.5% duty cycle chopper and a 50% one are used. A beam flag to switch the beam on and off is also present in the second stage. The third stage acts as a buffer chamber. The molecular beam is generated by a supersonic expansion of a gas mixture of oxygen and helium from an 80 μm

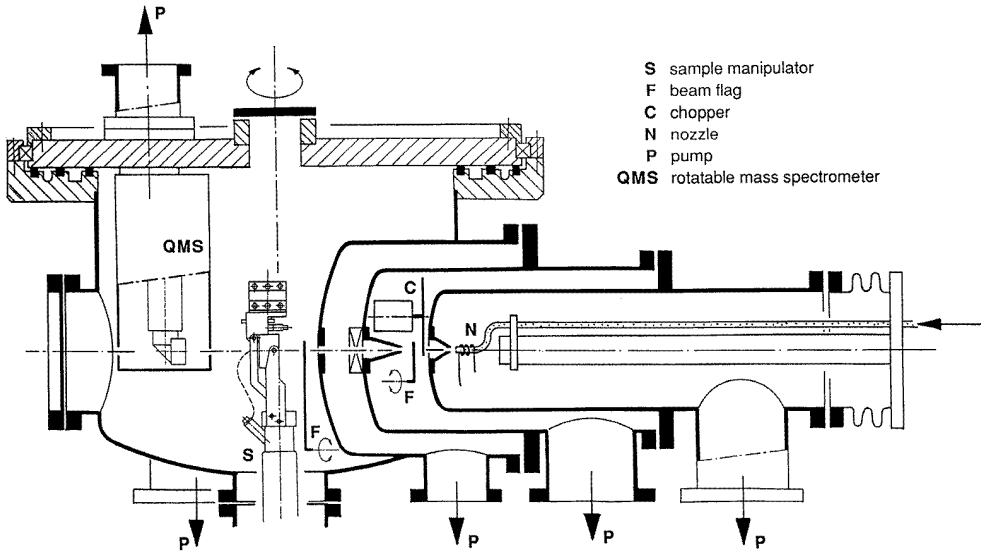

Figure 1. An overview of the experimental set-up. It shows the molecular beam line, consisting of three pumping stages, connected to a UHV chamber in which the sample is mounted on a sample manipulator. The cover of the UHV chamber, to which a differentially pumped mass spectrometer is connected, can be rotated.

CW quartz nozzle. By changing the oxygen/helium ratio in the gas mixture and heating the nozzle, we can vary the translational energy of the oxygen molecules from thermal to about 1.8 eV. Electronic flow controllers control the flows of oxygen and helium.

The sample is mounted in the middle of the UHV chamber on a three-axis goniometer [14]. A quadrupole mass spectrometer (QMS) can be rotated around the sample to detect the particles leaving the surface after desorption or scattering. Combining the movements of the manipulator and the rotatable QMS gives accurate control (by computer) over the angles θ_i, ϕ_i, θ_f and ϕ_f. θ_i is the incidence angle and is measured with respect to the surface normal, ϕ_i is the azimuthal angle of the incident particle measured with respect to the $\langle 1\bar{1}0 \rangle$ azimuthal direction on the surface, θ_f is the scattering angle measured with respect to the surface normal and ϕ_f is the angle of the scattered particle measured with respect to the incidence plane. By moving the sample out of the beam, the TOF of the direct beam can be recorded. In this way the translational energy of the oxygen molecules is derived for the different nozzle temperatures and flow settings. Liquid nitrogen cooling allows a minimum sample temperature of approximately $T_s = 160$ K to be achieved. The sample temperature is measured with a thermocoax K-type thermocouple inserted in the side of the sample and is controlled by a commercial controller. The controller allows linear ramping of the sample temperature employed in this study for the temperature-programmed desorption (TPD) measurements

A residual-gas analyser (RGA) is present for monitoring the background gas and an ion sputter gun for cleaning the sample. The RGA has been calibrated for the absolute oxygen partial pressure rise in the system [8]. Monitoring the background pressure gives values for incident flux and desorption rates in the TPD experiments. Surface coverages can be given since the surface area covered by the molecular beam ($9.5/\cos\theta_i$ mm$^2 \pm 5\%$) is known and are in accord with observed LEED patterns [8].

The samples are cut by spark erosion from a single-crystal rod of 5N purity to within 0.1° of the (110) plane and polished by standard polishing techniques. Once in UHV the sample received a treatment of sputtering (500 eV Ar^+ ions, $T_s = 600$ K) and annealing ($T_s = 800$ K) cycles until the angular width of the specularly reflected He intensity was approximately 2°, which is the angular resolution of our experiment. For He scattering along the ⟨001⟩ azimuth of the surface, which is the corrugated direction, we could measure the second-order diffraction peak and at least 25% of the incident He flux could be accounted for in the detected scattered flux. To further check the surface quality, the system is also equipped with LEED and AES.

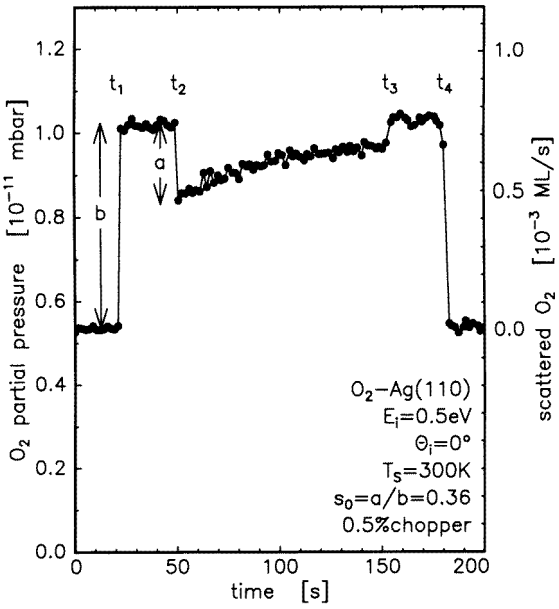

Figure 2. An oxygen partial pressure trace displaying the method of King and Wells for measuring the sticking probability. The left-hand axis shows the oxygen partial pressure in the system and the right-hand axis the number of molecules reflected from the incident molecular beam.

Sticking probabilities above 0.05 are measured with the method of King and Wells [15]. In this method the partial pressure of the reactive gas is monitored in time. A partial pressure trace for O_2 is shown in figure 2. Before t_1 the beam is prevented from entering the UHV chamber by closing the beam flag in the beam line (see figure 1). The partial pressure measured is the residual oxygen pressure of the system. Then the beam is allowed to enter the UHV chamber at time t_1 by opening the flag in the beam line, but it is not allowed to hit the sample by keeping the flag in the UHV chamber closed. The observed pressure rise is proportional to the incident flux of O_2 molecules. Upon opening the UHV beam flag at time t_2, the partial pressure will drop due to oxygen sticking to the surface and the partial pressure decrease is proportional to the number of molecules that stick to the surface. Taking the ratio of pressure drop and pressure rise, denoted as a and b, respectively, in figure 2, yields the initial sticking probability. The pressure increase after the sharp drop reflects a decrease in sticking with increasing surface coverage. By integrating the pressure drop one can obtain the sticking coefficient as a function of the surface coverage. No increase in

pressure is observed when the beam is allowed to hit the (inert) UHV flag, which indicates that no adsorption occurs at this beam flag. At times t_3 and t_4 the UHV flag and the flag in the beam line are closed, respectively. The left-hand axis of figure 2 is the partial oxygen pressure expressed in mbar. It shows that the pressure increase in the system due to the oxygen in the beam (0.5% chopper) is in the 10^{-12} mbar range. The right-hand axis shows the number of oxygen molecules that scatter from the surface and thus contribute to the partial pressure rise in the system. It is expressed as the number of molecules hitting the area occupied by one Ag atom at the Ag(110) surface (11.8 $\mathrm{\AA}^2$) per second. The surface may in this case be either the UHV flag or the sample surface. We employed the 0.5% duty cycle chopper for these measurements to reduce the average flux entering the UHV chamber and incident on the surface, to minimize the error due to the vacuum time constant of the UHV system.

Sticking probabilities below 0.05 were measured using the 50% chopper by determining the ratio of molecules that have stuck to the surface and the oxygen dose at the surface in the limit of zero coverage. The oxygen dose is derived by integrating the partial pressure rise in the system during dosing and the number of molecules that have stuck by measuring and integrating a TPD spectrum after adsorption [8]. The sensitivity of the RGA should be kept identical for the two measurements.

For the TOF experiments, the flight time of the oxygen molecule was measured from the 0.5% duty cycle chopper in the beam line to the rotatable QMS. The delay between the time pick-off from the chopper blade and the passing of the beam is calibrated by varying the chopper rotation speed. Detected particles, marking the end of the TOF, were counted by a home-built multichannel scaler in 2 μs bins. In analysing the TOF spectra, the ion flight time through the QMS was subtracted from the TOF time axis. The recorded TOF spectra are fitted to shifted Maxwell–Boltzmann distributions convoluted over the finite chopper opening time which yields the mean energy per particle $\langle E_\mathrm{i} \rangle$ in the beam [16, 17]. From the TOF distributions of both the incident and scattered particles a relative value for incident and scattered flux can be found and also the mean values for the energy $\langle E \rangle$ of the incident and scattered or desorbing particles. The scattered flux is corrected for the incident flux. In the text $\langle E \rangle$ will be replaced by E.

3. Results and discussion

Results on scattering, sticking and desorption of O_2 for the Ag(110) surface will be presented. Scattering and sticking has been done along both the $\langle 1\bar{1}0 \rangle$ and the $\langle 001 \rangle$ azimuths. Sticking and desorption measurements are done for the dissociated state only, since we could not reach a low enough surface temperature T_s to isolate the molecular chemisorption state at the surface.

3.1. Oxygen scattering

Angularly resolved scattering results expressed in scattered flux and in the ratio of the energy of the molecule after the collision E_f and the incidence energy E_i are shown in figures 3 and 4 for different E_i at a fixed T_s and for different T_s at a fixed E_i, respectively. All scattering measurements were carried out in the plane of incidence ($\phi_\mathrm{f} = 0^\circ$) and for $\theta_\mathrm{i} = 40^\circ$. The left-hand panels show the results for scattering along the $\langle 1\bar{1}0 \rangle$ azimuth and the right-hand panels for the scattering along the $\langle 001 \rangle$ azimuth. To prevent the uptake of dissociated oxygen at a T_s below the recombinative desorption temperature of $T_\mathrm{s} \approx 600$ K, we increased the background CO partial pressure to 2×10^{-7} mbar during the experiments

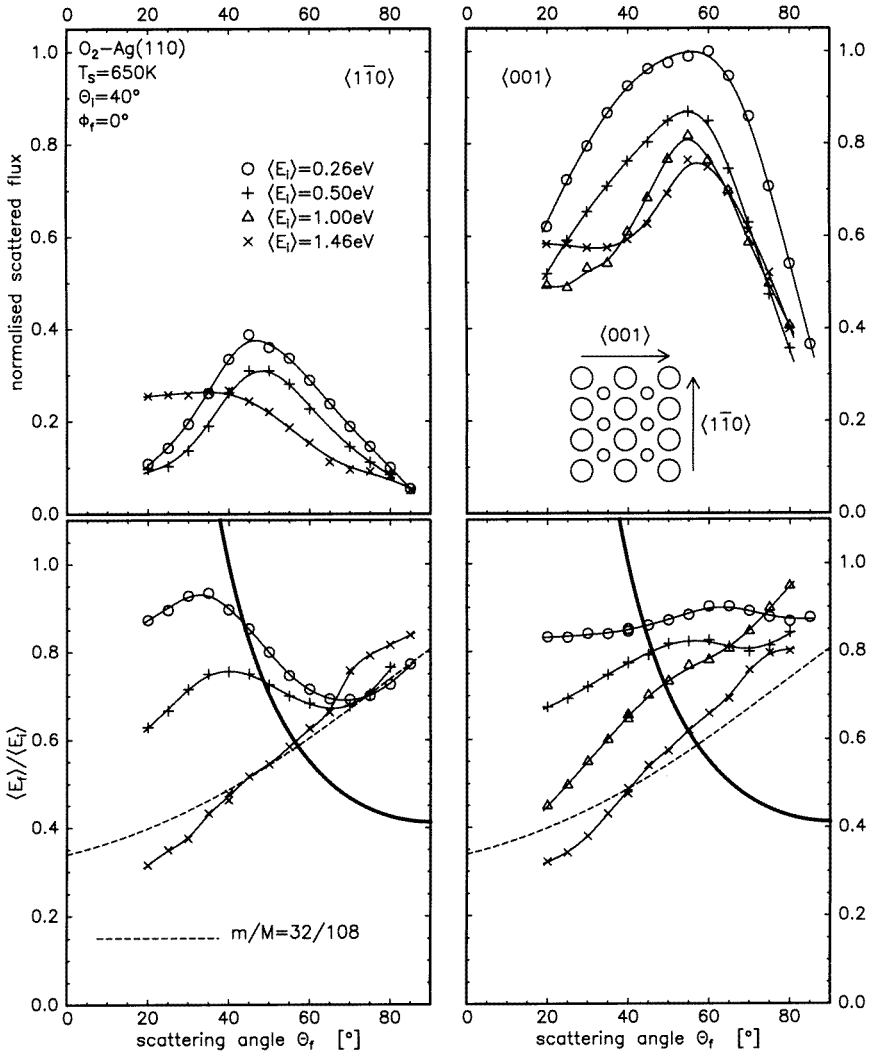

Figure 3. Angularly resolved energy (bottom panels) and flux (top panels) distributions of O_2 molecules scattered from the Ag(110) surface for $\theta_i = 40^\circ$, $T_s = 650$ K and several E_i. The lines through the data points are to guide the eye only. The thick line in the lower panels holds for parallel momentum conservation and the dashed line for hard-sphere scattering. The left-hand panels show scattering along the $\langle 1\bar{1}0\rangle$ azimuth and the right-hand panels scattering along the $\langle 001\rangle$ azimuth. A top view of the Ag(110) surface is shown in the top right-hand panel with the small circles representing the second-layer atoms.

to react the adsorbed oxygen off, forming CO_2. Below $T_s = 300$ K, the silver surface becomes covered with a carbonate species in this process, as has been observed before [3, 18], preventing scattering experiments below this surface temperature. The top panels of both figures show the scattered relative flux normalized to the maximum scattered relative flux value found, which is for $E_i = 0.26$ eV along the $\langle 001\rangle$ azimuth. It is observed that the scattered flux detected along the $\langle 1\bar{1}0\rangle$ azimuth is considerably lower than that detected along the $\langle 001\rangle$ azimuth. The bottom panels of both figures show the energy ratios E_f/E_i

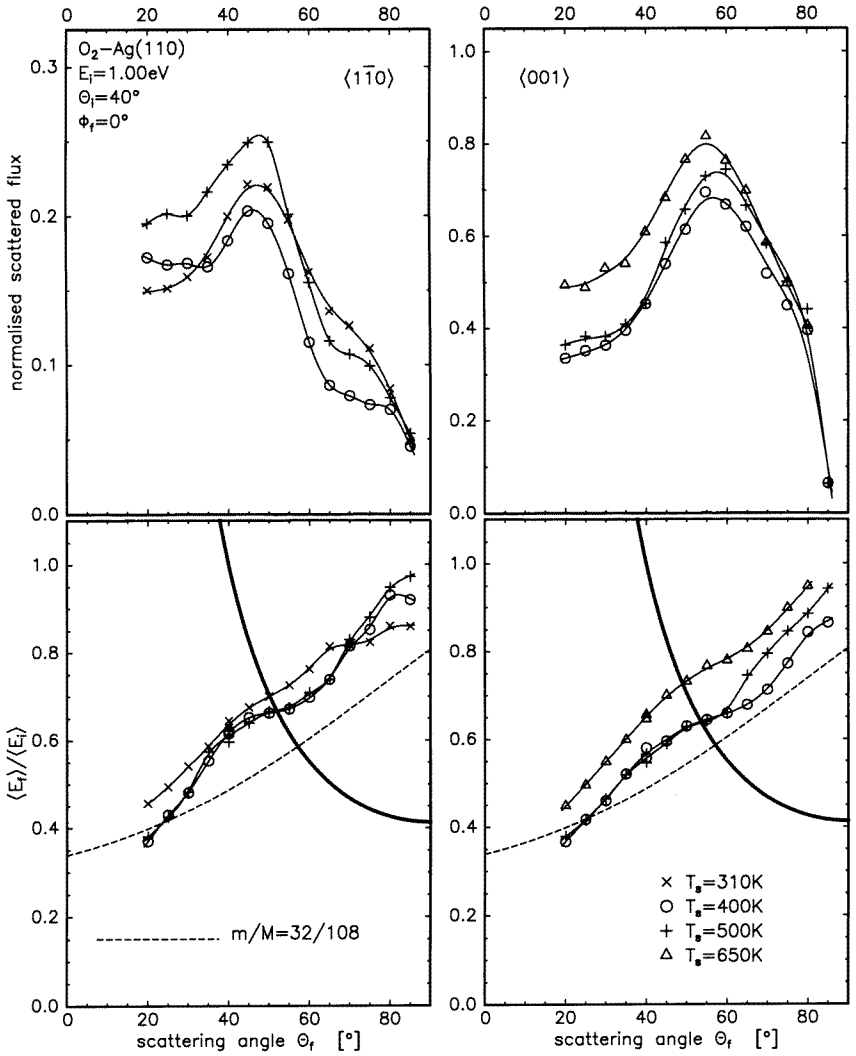

Figure 4. Angularly resolved energy (bottom panels) and flux (top panels) distributions of O_2 molecules scattered from the Ag(110) surface for $\theta_i = 40^\circ$, $E_i = 1.00$ eV and several T_s. The lines through the data points are to guide the eye only. The thick line in the lower panels holds for parallel momentum conservation and the dashed line for hard-sphere scattering. The left-hand panels show scattering along the $\langle 1\bar{1}0 \rangle$ azimuth and the right-hand panels scattering along the $\langle 001 \rangle$ azimuth.

for the scattered molecules. The thick line is according to parallel momentum conservation in the collision and the dashed line according to a binary collision ('hard-sphere scattering') of a mass 32 (O_2) with a mass 108 (Ag) [5].

Turning our attention first to figure 3, one observes that scattering along the $\langle 001 \rangle$ azimuth results in a broader angular flux distribution for the different E_i, especially true for low E_i. The maximum in the distribution has also shifted further away from the specular direction towards the surface. Scattering along this azimuth means scattering across the rows on the Ag(110) surface and thus along the most corrugated direction on this surface.

However, it does not lead to less detected scattered flux than for scattering along the rows (the $\langle 1\bar{1}0\rangle$ azimuth). We attribute the observed difference in scattered flux intensity along the two azimuths to a defocusing of the flux for scattering along the $\langle 1\bar{1}0\rangle$ azimuth. This defocusing has been observed for ion scattering along this orientation [19, 20], when the ion is incident 'on top' of the rows. A weak focusing was observed for ions incident in the grooves. An O_2 molecule is easily scattered away from the plane of incidence if it is incident along the rows of the surface corrugation and a broader out-of-plane intensity distribution than for the $\langle 001\rangle$ azimuth should be the case. We have not carried out such an out-of-plane measurement. A difference in sticking probabilities cannot account for the difference in the intensities of observed scattered flux since they only show a relative difference of approximately 16% and sticking is even larger for the $\langle 001\rangle$ azimuth as will be shown later. The observed broader intensity distributions in the incidence plane should also lead to a decrease of the maximum intensity. For the largest E_i, the scattered flux is observed to have increased for subspecular scattering angles.

The shape of the angular distributions along the $\langle 001\rangle$ and $\langle 1\bar{1}0\rangle$ azimuths is very different and is due to the different corrugation. Helium scattering shows only specular scattering along the $\langle 1\bar{1}0\rangle$ azimuth [21, 22]. Scattering along this azimuth is quite similar for both He and O_2 to scattering from the Ag(111) crystal [5]. A peak around the specular direction is observed with a shoulder towards smaller θ_f. The specular peak may be due mostly to scattering from the bottom of the flat $\langle 1\bar{1}0\rangle$ grooves (from the second-layer atoms). The shoulder may be due to the enhanced local, hard-sphere-like corrugation as is also seen for Ag(111) and due to zigzag multiple collisions in the grooves. Along the $\langle 001\rangle$ azimuth, He scattering shows three diffraction peaks [21], which indicates a corrugation of the surface. It should be noted that no rainbow scattering is observed and that the corrugation is not very strong [23, 24]. The O_2 scattering shows a pronounced broadening and a shift of the peak position towards the surface. This is indicative for a much stronger corrugation. Such an effect has been observed for Cl_2 scattering from Ag(111) [25], NO scattering from Pt(111) [26, 27] and O_2 scattering from W(110) [28]. The shift in the present case is stronger. Kara and DePristo performed calculations of the angular distributions for N_2 scattered from W(110) and a similar shift to that in the present work was found [29]. The potential energy surface used in these calculations shows a strong corrugation of the surface and was designed to explain the scaling of the probability of sticking of N_2 on W(110) with total rather than normal energy. The resemblance clearly indicates that the potential along the $\langle 001\rangle$ direction is corrugated.

The energy transfer is also quite different along the two azimuths except at the highest E_i of 1.46 eV. For this E_i, the energy ratio curve follows the hard-sphere scattering line quite closely and the scattered molecules must have experienced a very corrugated surface in both cases. At the lower E_i, the energy ratio curves for the $\langle 1\bar{1}0\rangle$ azimuth show some resemblance around the specular direction to the curve for parallel momentum conservation. As we also observed for scattering from the Ag(111) surface, some of the incident flux experiences a rather flat surface and another part a more corrugated surface [5]. This is not the case for the $\langle 001\rangle$ azimuth. No indication for parallel momentum conservation is observed. The energy ratio curves are observed to shift upwards and to run horizontal for decreasing E_i. For $E_i = 0.26$ eV, the energy ratio curve is almost constant over θ_f and displays that approximately 85% of E_i is conserved in the collision. This is a larger value than the one found for the scattered flux along the other azimuth or for O_2 scattering from the Ag(111) surface. It shows that for scattering along the $\langle 001\rangle$ azimuth at low E_i, the scattering process is remarkably different from both parallel momentum conservation and the binary collision model.

Changing T_s for both azimuths and for $E_i = 1.00$ eV does not have a drastic effect on the energy transfer as can be seen in figure 4. For the $\langle 001 \rangle$ azimuth, the scattered flux increases at subspecular angles and for the $\langle 1\bar{1}0 \rangle$ azimuth a slight overall change is observed. The most striking observation in the scattered flux distributions is the sharp drop in intensity at $\theta_f = 80^\circ$. It is observed for both azimuths, but is most pronounced for the $\langle 1\bar{1}0 \rangle$ azimuth. The feature at $\theta_f = 80^\circ$ along the $\langle 1\bar{1}0 \rangle$ azimuth may be due to the preferential focusing of molecules along the grooves discussed above.

Sticking of O_2 in the molecular chemisorption state can reach a probability of up to 50%, exceeding the probability for dissociative chemisorption at these T_s. Desorption from this state should be visible in the measured TOF spectra. At $T_s = 650$ K, desorption from the dissociated state can also occur. However, the maximum dissociation probability of 5% and the long surface residence time compared to the time-scale of the TOF at this T_s will make desorption from the latter state invisible in the TOF spectra. For scattering of O_2 from the Ag(111) surface, we did not observe desorption from the molecular chemisorbed state since the corresponding sticking probability is too low ($<10^{-3}$). Instead, we observed transient trapping–desorption of O_2 molecules, with a sharply peaked desorption distribution around the surface normal [6, 7]. This may also occur at the Ag(110) surface.

The occurrence of desorption features is not obvious from the TOF spectra measured for the O_2–Ag(110) system. A single shifted Maxwell–Boltzmann distribution seems sufficient to make a good fit to the TOF spectra. No desorption of molecules according to a non-shifted Maxwell–Boltzmann distribution with a temperature close to T_s is observed. Still, adsorption–desorption from the molecular state should have a large probability. It may be that the desorbing molecules have superthermal energies due to a barrier in the desorption path above the vacuum zero level or that the molecules have not completely thermalized in the molecular well. The transient species observed on Ag(111) displayed a strong dependence on T_s and was only well resolved below $T_s = 300$ K. The results shown in figures 3 and 4 are obtained by fitting one shifted Maxwell–Boltzmann distribution to the measured TOF spectra.

3.2. Oxygen sticking

Figures 5, 6 and 7 display the initial dissociative sticking probability $s_{D,0}$ measured as a function of E_i, θ_i, ϕ_i and T_s. $s_{D,0}$ shows an increase with increasing E_i up to $E_i \approx 0.75$ eV, which agrees very well with the measurements of Vattuone *et al* (see [9, 30]).

$s_{D,0}$ is observed to increase with decreasing T_s as was also observed by Vattuone *et al*. This T_s-dependence is explained by first sticking into the molecular chemisorption state followed by dissociation via a thermal process. With a subscript $_D$ we will refer to the dissociated state and with a subscript $_M$ to the molecular state. Since $s_{D,0}$ is governed by the competition between desorption and dissociation from the molecular state, it is given by the ratio of the rate constant for dissociation and the sum of rate constants for dissociation and desorption and can be written as

$$s_{D,0} = \frac{s_{M,0}\, k_{M,diss}}{k_{M,diss} + k_{M,des}} = s_{M,0}\left[1 + \frac{\nu_{M,des}}{\nu_{M,diss}} \exp\left(-\frac{E_{M,des} - E_{M,diss}}{k_B T_s}\right)\right]^{-1} \qquad (1)$$

with the rate constant given by

$$k = \frac{1}{\tau} = \nu \exp\left(-\frac{E}{k_B T_s}\right) \qquad (2)$$

where $\nu_{M,des}$ and $\nu_{M,diss}$ are the prefactors for desorption and dissociation, $E_{M,des}$ and $E_{M,diss}$ the activation energies for desorption and dissociation from the molecular chemisorption

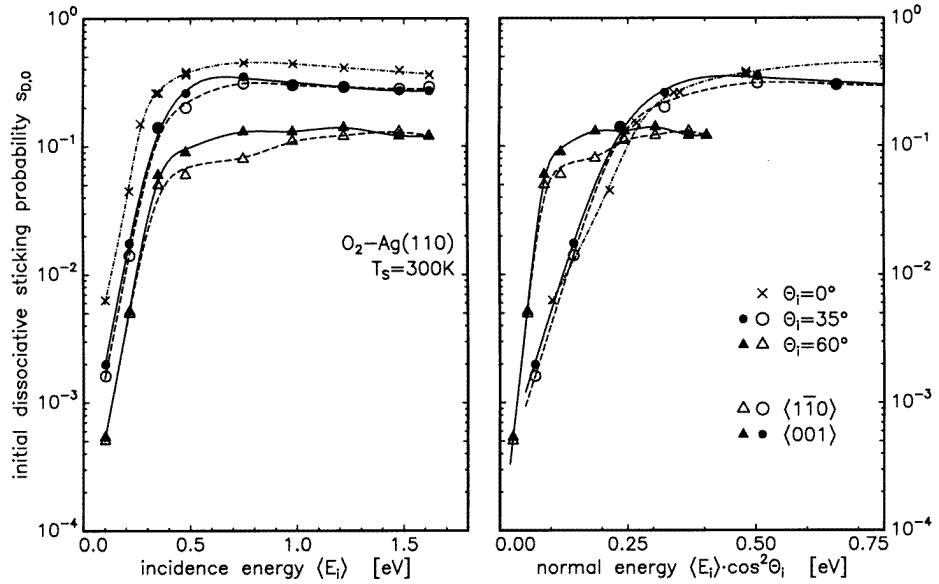

Figure 5. The dissociative sticking probability as a function of both total and normal-incidence energy for different θ_i along both the $\langle 1\bar{1}0 \rangle$ and $\langle 001 \rangle$ azimuths. Lines through the data points are to guide the eye only.

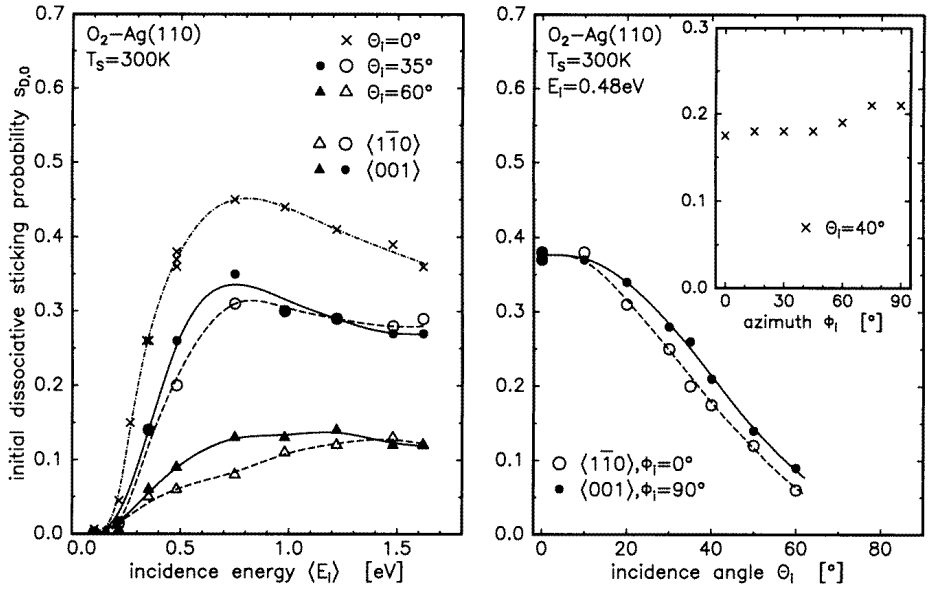

Figure 6. The dissociative sticking probability as a function of E_i is displayed in the left-hand panel for several θ_i along both azimuthal directions. The right-hand panel shows the θ_i-dependence for one E_i and the inset shows the dissociative sticking probability when varying the azimuthal angle. Lines through the data points are to guide the eye only.

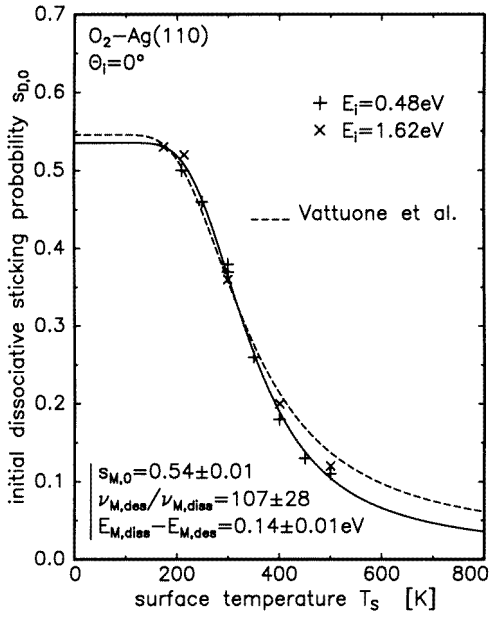

Figure 7. The dissociative sticking probability as a function of T_s for two different E_i. The full line is a fit of equation (1) to the data. The dashed line is according to the data of Vattuone *et al* [9].

state, $s_{M,0}$ the initial sticking probability into the molecular chemisorption state and k_B Boltzmann's constant. The full line shown in figure 7 is a fit to the data according to this model. All values except $s_{M,0}$ are expected to be equal for the data for both E_i shown. It is a pure coincidence that the data for the two E_i exactly coincide, meaning that $s_{M,0}$ is equal for both E_i. The value found for $s_{M,0}$ at $E_i = 0.49$ eV is equal to the one reported by Vattuone *et al*. The values for the difference in desorption energies and the ratio of prefactors differ slightly from the ones found by Vattuone *et al*: $\nu_{M,des}/\nu_{M,diss} = 107 \pm 28$ as opposed to 40 and $E_{M,des} - E_{M,diss} = 0.14 \pm 0.01$ eV as opposed to 0.112 eV for our results and the results of Vattuone *et al*, respectively. The dashed line in figure 7 is according to the results of Vattuone *et al*. The initial molecular sticking probability $s_{M,0}$ as a function of E_i and θ_i has been measured directly by Vattuone *et al* [9] and Rocca *et al* [13] and is identical to the dependence of $s_{D,0}$ on these parameters for E_i up to 0.8 eV. This observation and the T_s-dependence found by Vattuone *et al* and us below and above $E_i = 0.8$ eV indicates that dissociation is preceded by molecular chemisorption. No other model is available to explain this behaviour.

Figure 6 shows $s_{D,0}$ for several θ_i along different azimuthal directions. It is clearly observed that an azimuthal dependence is present in the sticking as was first reported by Vattuone *et al* [10]. The largest absolute difference between the $\langle 1\bar{1}0 \rangle$ and the $\langle 001 \rangle$ azimuth observed is approximately 0.05. A variation of $s_{D,0}$ with the azimuth varied in small steps is shown in the inset of the right-hand panel. $s_{D,0}$ for the different θ_i and both azimuths is also shown in figure 5 on a logarithmic scale as a function of both total and normal-incidence energy. It is observed that the azimuthal dependence is most pronounced between $E_i \approx 0.3$ eV and $E_i \approx 1.2$ eV. Above and below this E_i-interval, the probabilities for the two azimuths are almost identical. In figure 5 it is obvious that the energy scaling of the

dissociative sticking is between total energy and normal energy scaling. From the plot of $s_{D,0}$ on a linear scale as a function of total energy E_i (the left-hand panel of figure 6) an energy threshold of approximately 0.2 eV is observed. For the Ag(111) surface, a value of 0.2 eV was found as a threshold in the normal-incidence energy ($E_i \cos^2 \theta_i$) for an increase in surface corrugation and for transient trapping and molecular and dissociative sticking to occur [5, 6, 7, 8]. Sticking and scattering is almost identical along the $\langle 1\bar{1}0 \rangle$ and the $\langle 001 \rangle$ azimuth for $E_i > 1$ eV and is explained by the interaction of the O_2 molecule with primarily one Ag atom for these E_i. The right-hand panel of figure 6 shows the decrease in $s_{D,0}$ for $E_i = 0.48$ eV with increasing θ_i for both azimuthal directions.

For the O_2–Ag(111) system, a second process for dissociative sticking was found above $E_i \approx 1$ eV and $\theta_i < 60^\circ$ [8]. However, even the increase in $s_{D,0}$ due to this process resulted only in a maximum value of 2×10^{-3}. This process, which was attributed to a direct dissociation channel, may also be present for the O_2–Ag(110) but is not visible because the observed indirect dissociation process is three orders of magnitude larger than for the Ag(111) surface.

We have also studied the dissociative sticking as a function of the surface coverage ψ_D. It is found that s_D is initially rapid followed by a slower uptake for ψ_D above approximately 0.08 ML. The sticking probabilities reported above were the initial sticking probabilities and hold for this 'fast'-uptake regime. After this first uptake regime the sticking probability drops to a value of the order of 10^{-4}. These results will be published in a separate paper [31].

3.3. Recombinative oxygen desorption

The asymmetric shape of the TPD spectra suggests that the desorption is first order in ψ_D. If this is the case then the maximum desorption temperature should not shift for different initial ψ_D. Figure 8 shows different TPD spectra taken at an equal heating rate β and different initial ψ_D. A dramatic positive shift in the peak desorption temperature of 15 K is observed with increasing ψ_D as is shown in figure 9. The peak shift reaches a saturation at $T_s \approx 587$ K for initial coverages above $\psi_D = 0.25$ ML. This surface coverage corresponds to a (4×1) structure. A peak shift with ψ_D was also observed by Bowker, Barteau and Madix [32].

The left-hand panel of figure 10 shows TPD spectra taken at different β and initial ψ_D larger than 0.25 ML. The peak desorption temperature is in this case independent of the initial ψ_D. Assuming first-order desorption, from the slope of $\ln(T_{peak}^2/\beta)$ versus $1/T_{peak}$, as is shown in the right-hand panel, a value for the desorption energy $E_{D,des}$ is found. The peak desorption temperature T_{peak} varies over a larger range than for recombinative O_2 desorption from the Ag(111) surface [8]. Using the value found for $E_{D,des}$ in the equation for first-order desorption yields a value for the prefactor $\nu_{D,des}$. The values found from this analysis are $E_{D,des} = 1.73 \pm 0.05$ eV and $\nu_{D,des} = 10^{14.0\pm0.4}$ s^{-1}. However, simulating the TPD spectra assuming first-order desorption using these values leads to simulated spectra which are much broader than the measured TPD spectra [17]. Clearly, a simple first-order picture is too simple.

Second-order desorption kinetics is expected for recombinative desorption of a diatomic molecule, unless adsorbate interactions play a role. In this case, the TPD spectra may appear first-order like. Bowker [33] simulated the recombinative O_2–Ag(110) TPD spectra of Bowker *et al* [32] using a function described by King [34], which takes lateral interactions into account. These simulations showed a peak shift to higher T_s with increasing initial ψ_D and described the data very well. The values of the parameters used were $E_{D,des} = 1.52$ eV, $\nu_{D,des} = 4\times10^{14}$ s^{-1} and 0.145 eV for the adsorbate attractive interaction energy. It was

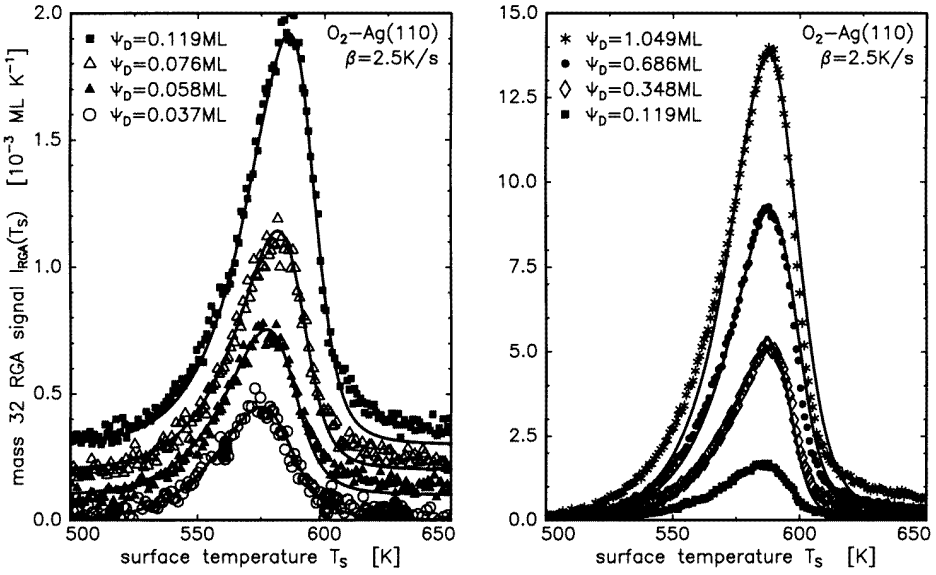

Figure 8. TPD spectra taken for different initial coverages Ψ_D at equal heating rate β. The full lines are from a simulation according to the formalism of Zhdanov with $\nu_{D,des} = 10^{15}$ s^{-1}. The values of the parameters are shown in table 1.

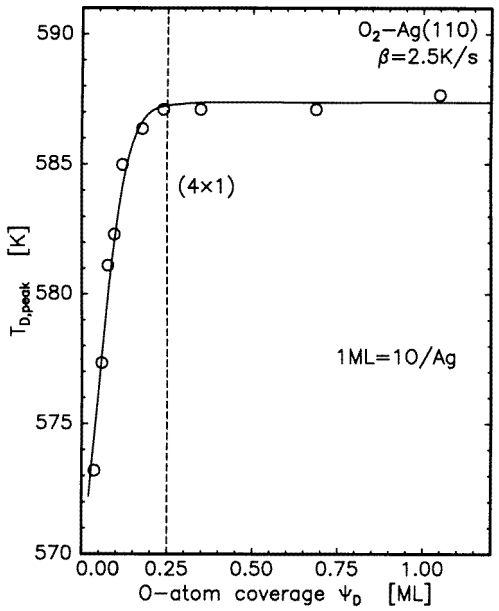

Figure 9. The peak temperature of TPD spectra taken at equal β for different Ψ_D. Most corresponding TPD spectra are shown in figure 8. The line through the data points is to guide the eye only.

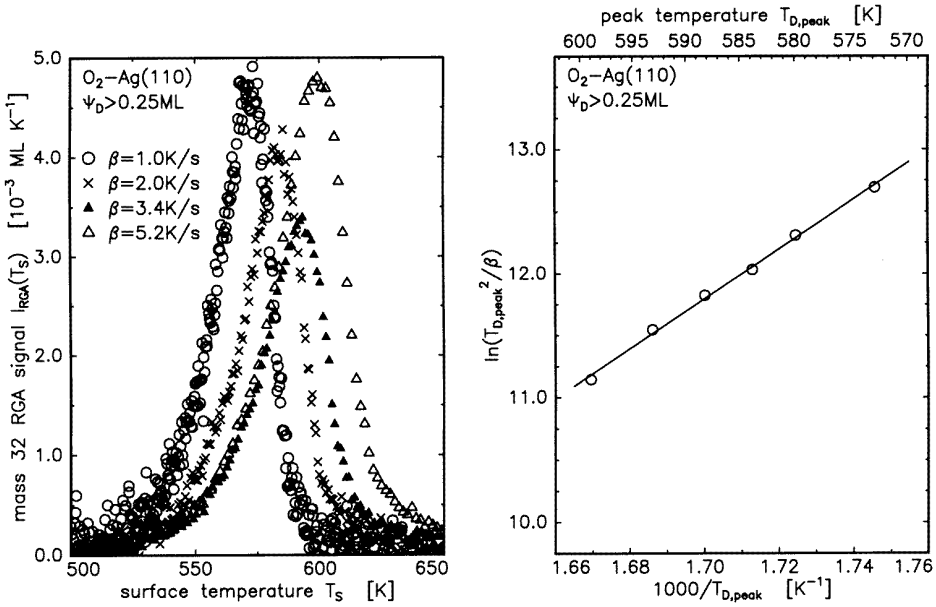

Figure 10. The left-hand panel shows TPD spectra for different β, and from the slope of the linear dependence shown in the right-hand panel a value for $E_{\mathrm{D,des}}$ can be found.

pointed out that the latter is a net interaction energy equivalent to the sum of attractive and repulsive interactions.

Table 1. Parameters in the Zhdanov formalism which give the best correspondence to the measured data. The metal–metal interaction is kept fixed at $\varepsilon^{x}_{\mathrm{MM}} = -0.01$ eV.

		$\nu_{\mathrm{D,des}} = 10^{14}$ s^{-1}		$\nu_{\mathrm{D,des}} = 10^{15}$ s^{-1}	
β	Ψ_{D}	$E_{\mathrm{D,des}}$	$\varepsilon^{x}_{\mathrm{AA}}$	$E_{\mathrm{D,des}}$	$\varepsilon^{x}_{\mathrm{AA}}$
2.5 K s^{-1}	0.037 ML	1.600 eV	−0.190 eV	1.715 eV	−0.180 eV
	0.058	1.600	−0.190	1.715	−0.190
	0.076	1.605	−0.190	1.723	−0.180
	0.119	1.615	−0.170	1.732	−0.160
	0.348	1.610	−0.135	1.732	−0.125
	0.686	1.640	−0.075	1.760	−0.065
	1.049	1.655	−0.050	1.780	−0.040
1.0 K s^{-1}	0.320 ML	1.605 eV	−0.145 eV		
2.0	0.300	1.610	−0.145		
3.4	0.265	1.615	−0.145		
5.2	0.375	1.610	−0.130		

Another option is the formalism given by Zhdanov [35] to simulate the measured TPD spectra. In this formalism, both an adsorbate–adsorbate interaction and a surface reconstruction are taken into account. The results of those simulations carried out to fit our data are the full lines shown in figure 8. In table 1, the parameters entering the formalism are displayed. The prefactor was fixed at either $\nu_{\mathrm{D,des}} = 10^{-15}$ s^{-1} or 10^{-14} s^{-1} and the

metal–metal attraction was kept fixed at $\varepsilon^x_{\mathrm{MM}} = -0.01$ eV for all the simulations. Varying the latter did not have a large effect on the simulated spectra and both prefactors led to fits of equal quality. It is observed that $E_{\mathrm{D,des}}$ increases and the adsorbate–adsorbate interaction $\varepsilon^x_{\mathrm{AA}}$ decreases with increasing initial ψ_{D}. A good correspondence between simulation and data is observed except for for the largest initial ψ_{D}. However, the Zhdanov model is not applicable to this initial ψ_{D} since a reconstruction other than an $(n \times 1)$ structure is involved [1]. The decrease in $\varepsilon^x_{\mathrm{AA}}$ with increasing initial ψ_{D} probably points to an increase in repulsive interactions for increasing ψ_{D}. The net interaction will therefore become less attractive for increasing ψ_{D}. The value found by Bowker [33] for the attractive interaction energy is in the range found by us.

Canepa *et al* [36] also applied the Zhdanov formalism to their TPD data and also found an increase in $E_{\mathrm{D,des}}$ with increasing ψ_{D}, but an increase in $\varepsilon^x_{\mathrm{AA}}$ with increasing ψ_{D}. For the TPD spectrum for $\psi_{\mathrm{D}} = 0.5$ ML, they found a decrease in the width of the TPD spectrum with respect to the spectra taken at lower ψ_{D}. This is in contrast to our data. Since we dosed with a molecular beam and they from a background gas, a different surface reconstruction may have formed giving rise to a different TPD spectrum. However, we have observed a (2×1) LEED pattern in the 0.5 ML range which is in agreement with their data and other data available [1]. It is also hard to imagine that the reconstruction formed is dependent on the dosing method. Another reason for the discrepancy may be that they detected O_2 molecules leaving the surface along the surface normal whereas we measured the integrated angular distribution.

Using the Zhdanov model, one can obtain simulated TPD spectra which agree very well with measurements. However, the values of the parameters in the model change with surface coverage. Improvements to the model are therefore suggested. At the moment, only an attractive interaction is included and no repulsive interaction to account for the spacing between the oxygen and silver rows. It should also be noted that experiments show an increase in the peak desorption temperature of the TPD spectra with increasing initial ψ_{D}. This trend is reproduced by the Zhdanov model for initial ψ_{D} exceeding 0.1 ML, but is reversed for lower initial ψ_{D}.

4. Sticking mechanisms

Comparing the results for the dissociative and molecular sticking of O_2 on Ag(111) with those on Ag(110), one observes that both surfaces show an increase in both sticking probabilities with increasing E_{i} and with approximately equal threshold energy. A maximum and a subsequent decrease in dissociative sticking is also observed for both the Ag(110) and Ag(111) surface planes. However, a difference of over two orders of magnitude in sticking probabilities is observed. For Ag(111), transient trapping of O_2 molecules is observed which is suggested to act as a precursor to molecular sticking. If transient trapping also occurs and acts as a precursor for the Ag(110) surface, the probability for equilibration of the transient species should be much higher. For the Ag(111) surface the transient has been connected to the $O_2^{\delta-}$ molecular precursor. The lifetime in the transiently trapped state was sufficiently long that it decays primarily through desorption, not through molecular chemisorption. Due to the strong similarity of the probability for molecular and dissociative chemisorption (*vide* figures 5 and 6 and work by Vattuone *et al* [9]) it is clear that molecular chemisorption acts as a precursor to dissociative adsorption. Therefore, we infer that at the Ag(110) surface transient trapping occurs, which is followed by rapid molecular chemisorption. The transfer from transient trapping to molecular chemisorption occurs so rapidly that even at high energies (>1 eV) molecular chemisorption occurs. The difference between the (111)

and (110) faces may be due to the fact that at (110) the electron density in the grooves may be higher, so bonding of $O_2^{\delta-}$ in the grooves occurs more readily [37]. By contrast, on the (111) face, bonding of $O_2^{\delta-}$ may be more difficult and involve defect sites. We note that in the calculations by Van den Hoek and Baerends [38] for O_2 dissociation on a Ag(110)-like cluster, the binding energy of the dissociated molecule (having an internuclear distance of 6 Å) is much less than the binding energy of two O adatoms as follows from TPD. This might be due to the fact that strong bonding is only obtained after formation of the Ag–O added rows. Very recently, this was also observed by Gravil *et al* [37]. Formation of such reconstructed surfaces may be much easier on the (110) than on the (111) face. STM studies of the oxidation of the Ag(111) face, preferably using dosing by fast molecular beams, may shed more light on this matter. It is clear from our work and the present STM studies that oxidation of Ag(110) and Ag(111) is a complex process involving both complex adsorption dynamics through the formation of $O_2^{\delta-}$ species and their subsequent dissociation involving imperfections at the surface [31].

Just as for the O_2–Ag(111) system, for the O_2–Ag(110) system no influence of the molecular physisorption well on the dissociative sticking is observed. Such an influence would show up as an increase in sticking for decreasing E_i.

5. Conclusion

It has been shown that the Ag(110) surface shows a different scattering behaviour for O_2 scattering and thus a different corrugation along the $\langle 001 \rangle$ and the $\langle 1\bar{1}0 \rangle$ azimuths up to $E_i \approx 1$ eV at $\theta_i = 40^\circ$. The corrugation is approximately equal for the two azimuths for $E_i > 1$ eV at $\theta_i = 40^\circ$ according to the energy transfer of the scattered molecules. Dissociative sticking probabilities are smaller along the $\langle 1\bar{1}0 \rangle$ azimuth for energies between $E_i \approx 0.3$ eV and $E_i \approx 1.1$ eV for $\theta_i = 40^\circ$ and $E_i \approx 1.3$ eV for $\theta_i = 60^\circ$. Hence the more corrugated surface, as observed by the incident molecule, leads to a larger sticking probability. A threshold of $E_i \approx 0.2$ eV in total translational energy is observed for the increase in the dissociative sticking. It is seen to proceed via the molecular chemisorption state. Desorption from the molecular state could not be distinguished in the TOF spectra. This may be due to a barrier in the desorption channel or to the influence of the transient O_2 state. An influence of the physisorption state on the dissociative sticking is not observed.

TPD spectra taken are analysed using a first-order desorption model and give values for the desorption energy and prefactor close to the ones found by taking adsorbate interactions and a surface reconstruction into account according to the model of Zhdanov. However, the parameters in this model are not constant for the different initial surface coverages.

Acknowledgments

This work is part of the research programme of the Stichting voor Fundamenteel Onderzoek der Materie (FOM, Foundation for Fundamental Research on Matter). The work was made possible by financial support from the Nederlandse Organisatie voor Wetenschappelijk Onderzoek (NWO, Dutch Organization for Advancement of Research) and the EOARD, under contract number F61708-94-C0012. DAB ackowledges support by the network on 'orientation in molecule–surface interactions' of the EU Science Plan, under contract number ERBSC1∗CT910721 and an EU institutional fellowship under contract number ERBCHBGCT940701.

References

[1] Besenbacher F and Nørskov J K 1993 *Prog. Surf. Sci.* **44** 5
[2] Campbell C T and Paffett M T 1984 *Surf. Sci.* **143** 517
[3] Campbell C T 1985 *Surf. Sci.* **157** 43
[4] Reijnen P H F, Raukema A, Van Slooten U and Kleyn A W 1991 *Surf. Sci.* **253** 24
[5] Raukema A, Dirksen R J and Kleyn A W 1995 *J. Chem. Phys.* **103** 6217
[6] Raukema A and Kleyn A W 1996 to be published
[7] Raukema A and Kleyn A W 1995 *Phys. Rev. Lett.* **74** 4333
[8] Raukema A, Butler D A, Box F M A and Kleyn A W 1996 *Surf. Sci.* **347** 151
[9] Vattuone L, Rocca M, Boragno C and Valbusa U 1994 *J. Chem. Phys.* **101** 713
[10] Vattuone L, Boragno C, Pupo M, Restelli P, Rocca M and Valbusa U 1994 *Phys. Rev. Lett.* **72** 510
[11] Vattuone L, Rocca M, Boragno C and Valbusa U 1994 *J. Chem. Phys.* **101** 726
[12] Vattuone L, Rocca M, Restelli P, Pupo M, Boragno C and Valbusa U 1994 *Phys. Rev.* B **49** 5113
[13] Rocca M, Vattuone L, Boragno C and Valbusa U 1994 *J. Electron Spectrosc. Relat. Phenom.* **64/65** 577
[14] Raukema A, De Jongh A P, Alberda H P, Boddenberg R, Giskes F G, De Haas E, Kleyn A W, Neerings H, Schaafsma R and Veerman H 1996 to be published
[15] King D A and Wells M G 1972 *Surf. Sci.* **29** 454
[16] Spruit M E M, Kuipers E W, Geuzebroek F H and Kleyn A W 1989 *Surf. Sci.* **215** 421
[17] Raukema A 1995 Dynamics of chemisorption *PhD Thesis* University of Amsterdam
[18] Backx C, DeGroot C P M, Biloen P and Sachtler W M H 1983 *Surf. Sci.* **128** 81
[19] McEachern R L, Goodstein D M and Cooper B H 1989 *Phys. Rev.* B **39** 10 503
[20] Adler D L and Cooper B H 1991 *Phys. Rev.* B **43** 3876
[21] Schinke R and Luntz A C 1983 *Surf. Sci.* **124** L60
[22] Luntz A C, Mattera L, Rocca M, Terreni S, Tommasini F and Valbusa U 1983 *Surf. Sci.* **126** 695
[23] Kleyn A W and Horn T C M 1991 *Phys. Rep.* **199** 191
[24] Rieder K H 1994 *Surf. Rev. Lett.* **1** 51
[25] Geuzebroek F H, Spruit M E M and Kleyn A W 1992 *Surf. Sci.* **271** 207
[26] Wiskerke A E and Kleyn A W 1995 *J. Phys.: Condens. Matter* **7** 5195
[27] Wiskerke A E, Taatjes C A, Kleyn A W, Lahaye R J W E, Stolte S, Bronnikov D K and Hayden B E 1993 *Chem. Phys. Lett.* **216** 93
[28] Rettner C T, DeLouise L A and Auerbach D J 1986 *J. Chem. Phys.* **85** 1131
[29] Kara A and DePristo A E 1988 *Surf. Sci.* **193** 437
[30] The E_i-values given by Vattuone *et al* are opproximately 30% too low due to a calibration error in their time-of-flight chain (M Rocca 1995 private communication).
[31] Butler D A, Raukema A and Kleyn A W 1996 *Surf. Sci.* at press
[32] Bowker M, Barteau M A and Madix R J, 1980 *Surf. Sci.* **92** 528
[33] Bowker M 1980 *Surf. Sci.* **100** L472
[34] King D A 1979 *CRC Crit. Rev. Solid State Mater. Sci.* **7** 167
[35] Zhdanov V P 1992 *Surf. Sci.* **277** 155
[36] Canepa M, Salvietti M, Traverso M and Mattera L 1995 *Surf. Sci.* **331–333** 183
[37] Gravil P A, White J A and Bird D M 1996 *Surf. Sci.* at press
[38] Van den Hoek P J and Baerends E J 1989 *Surf. Sci.* **221** L791